MIT Open Access Articles

Estimation of changes in instantaneous aortic blood flow by the analysis of arterial blood pressure

Massachusetts Institute of Technology

Title Page:

Estimation of Changes in Instantaneous Aortic Blood Flow by the Analysis of Arterial Blood Pressure

Tatsuya Arai[1], Kichang Lee[2], Robert P. Marini[2], Richard J. Cohen[2]

1. Aerospace Biomedical Engineering, Massachusetts Institute of Technology

2. Harvard-MIT Division of Health Sciences and Technology

Abbreviated title: Aortic Blood Flow Reconstruction from Blood Pressure Waveform

Correspondence:

Richard J. Cohen

45 Carleton St. E25-335

Cambridge, MA 02142

USA

Tel: 617-253-0009

Fax: 617-253-3019

Email: rjcohen@mit.edu

Abstract and key terms

The purpose of this study was to introduce and validate a new algorithm to estimate instantaneous aortic blood flow (ABF) by mathematical analysis of arterial blood pressure (ABP) waveforms. The algorithm is based on an auto-regressive with exogenous input (ARX) model. We applied this algorithm to diastolic ABP waveforms to estimate the auto-regressive (AR) model coefficients by requiring the estimated diastolic flow to be zero. The algorithm incorporating the coefficients was then applied to the entire ABP signal to estimate ABF. The algorithm was applied to six Yorkshire swine data sets over a wide range of physiologic conditions for validation. Quantitative measures of waveform shape (standard deviation, skewness, and kurtosis) as well as stroke volume (SV) and cardiac output (CO) from the estimated ABF were computed. Values of these measures were compared with those obtained from ABF waveforms recorded using a Transonic™ aortic flow probe placed around the aortic root. The estimation errors were compared with those using Windkessel model. The ARX algorithm achieved significantly lower errors in the waveform measures, SV, and CO than those obtained using a Windkessel model ($P<0.05$).

Key Terms— Aortic blood flow, arterial blood pressure, cardiac output, stroke volume

Abbreviations, symbols, and terminology

ABF: Aortic Blood Flow [L/min]

ABP: Arterial Blood Pressure [mmHg]

AR: Auto-regressive

ARX: Auto-regressive with exogenous input

Ca: Arterial Compliance [mL/mmHg]

CAP: Central Arterial Pressure [mmHg]

CO: Cardiac Output [L/min]

FAP: Femoral Arterial Pressure [mmHg]

MAP: Mean Arterial Pressure [mmHg]

PCM: Pulse Contour Methods

RAP: Radial Arterial Pressure [mmHg]

RNMSE: Root-Normalized Mean Squared Error [%]

SD: Standard Deviation

SV: Stroke Volume [mL]

TPR: Total Peripheral Resistance [mmHg min L-1]

τ: Characteristic time constant [sec]

Introduction

Aortic blood flow (ABF), defined as the instantaneous flow rate of blood across the aortic valve, is one of the most fundamental cardiovascular signals. The beat-to-beat integral of the ABF waveform yields stroke volume (SV), and the time average of ABF over many beats yields cardiac output (CO). Individual ABF waveforms reflect the detailed time dependence of ventricular contractions; however, ABF data are not currently clinically available. The availability of ABF data would be particularly valuable for the evaluation of the contractile function of the left ventricle during normal and abnormal beats and for optimizing pacing parameters during bi-ventricular pacing.

The most accurate currently available method for the continuous measurement of ABF, SV, and CO is the surgical placement of an ultrasonic flow probe (Transonics^{TM}) around the aortic root. The drawback of the flow probe is that it requires a highly invasive open-chest surgical procedure (11). Non-invasive methods include Doppler echocardiography, which requires a skilled technician to hold the probe at the correct angle on the patient's body. Thus, long-term, continuous measurement is not feasible with this method.

In this paper, we introduce a novel algorithm to continuously estimate beat-to-beat ABF waveforms by analysis of the arterial blood pressure (ABP) signal. The algorithm can continuously estimate ABF on a beat-to-beat basis less obtrusively than the aforementioned methods because ABP is readily accessible by minimally or non-invasive means. This algorithm models the arterial tree as a system with ABF input and ABP output. The algorithm involves an auto-regressive with exogenous input (ARX) model. The key feature of the algorithm is that ARX coefficients are estimated by applying it to a diastolic ABP waveform and forcing the estimated ABF to be zero during this period. Then, the algorithm incorporating the estimated coefficients is applied to the single ABP signal in order to estimate ABF on a beat-by-beat basis.

Method

A. Algorithm

Over a short time interval, the cardiovascular system can be described as a time-invariant system with an input of ABF (*F[n]*) and output of ABP (*P[n]*), as illustrated in Fig. 1.

Fig. 1. ARX model.

An ARX model can be used to relate the ABP values *P[n]* to the ABF values *F[n]*:

$$P[n] = \sum_{j=1}^{L} a[j] P[n-j] + \alpha F[n] + e[n] \qquad (1)$$

where the *a[j]* are the auto-regressive weighting coefficients, *L* is the coefficient length, α is the weighting coefficient for the exogenous input *F[n]* , and *e[n]* is noise. The ARX model can be re-written as

$$\alpha F[n] = P[n] - \sum_{j=1}^{L} a[j] P[n-j] + e[n] \qquad (2)$$

During diastole, ABF (system input) is approximately zero:

$$P[n] = \sum_{j=1}^{L} a[j] P[n-j] + e[n] \qquad (3)$$

Therefore, the weighting coefficients *a[j]* are AR coefficients, which can be obtained by solving the matrix equation (using MATLAB, The Mathworks Inc., Natick, MA) that involves data from multiple beats:

$$
\begin{bmatrix}
P_1[n] \\
P_1[n+1] \\
\vdots \\
P_1[n+N_1-1] \\
\vdots \\
P_{17}[n] \\
P_{17}[n+1] \\
\vdots \\
P_{17}[n+N_{17}-1]
\end{bmatrix}
=
\begin{bmatrix}
P_1[n-1] & \cdots & P_1[n-L] \\
P_1[n] & \cdots & P_1[n-L-1] \\
\vdots & \ddots & \vdots \\
P_1[n+N_1-2] & \cdots & P_1[n-L+N_1-1] \\
\vdots & & \\
P_{17}[n-1] & \cdots & P_{17}[n-L] \\
P_{17}[n] & \cdots & P_{17}[n-L-1] \\
\vdots & \ddots & \vdots \\
P_{17}[n+N_{17}-2] & \cdots & P_{17}[n-L+N_{17}-1]
\end{bmatrix}
\begin{bmatrix}
a[1] \\
a[2] \\
\vdots \\
a[L]
\end{bmatrix}
\qquad (4)
$$

where the $P_i[n]$ are the ABP values in the ith beat and N_i is the number of diastolic samples in the ith beat ($1<$ $i < M$), where M is the number of beats in the moving window. An M = 17 moving window size was empirically found to be optimal and was therefore adopted. Note that the elements of the vector item on the left of Eq. 4 are diastolic ABP values. The typical AR coefficients $a[j]$ obtained by Eq. 4 are shown in Fig. 2a.

(a) AR coefficients

(b) Impulse response

Fig. 2. Typical AR coefficients $a[j]$ obtained by the algorithm (a) and impulse response $h[n]$ (b) obtained by Eq. 8 using the portion of the RAP signal in Swine #4.

The time constant was obtained from the exponential decay between two to four seconds. The coefficients and impulse response were obtained on a beat-by-beat basis.

The coefficient α can be also obtained on a beat-by-beat basis by the following procedure. By taking the average of both sides of Eq. 2:

$$\alpha = \left(1 - \sum_{j=1}^{L} a[j]\right) MAP/CO \qquad (5)$$

where MAP is mean arterial pressure. *MAP/CO* can be obtained from Ohm's law:

$$MAP/CO = TPR \qquad (6)$$

where TPR is total peripheral resistance. TPR can be related to the arterial compliance C_a and the characteristic time constant of the system τ:

$$\tau = C_a \times TPR \qquad (7)$$

where τ can be obtained by analyzing the exponential decay curve of the impulse response of the system *h[n]* (Fig. 2b):

$$h[n] = \sum_{j=1}^{L} a[j]h[n-j] + \alpha\delta[n] \qquad (8)$$

Equations 5-7 can be combined to compute α:

$$\alpha = \tau\left(1 - \sum_{j=1}^{L} a[j]\right)/C_a \qquad (9)$$

Therefore, using Eq. 1 and 9, instantaneous ABF can be expressed as:

$$F[n] = \frac{C_a}{\tau\left(1 - \sum_{j=1}^{L} a[j]\right)}\left(P[n] - \sum_{j=1}^{L} a[j]P[n-j]\right) \qquad (10)$$

The AR coefficient length *L* was chosen to minimize *Σa[j]* and updated on a beat-by-beat basis.

The integral of *F[n]* was calculated on a beat-to-beat basis to obtain proportional SV estimates (the proportionality constant is the unmeasured C_a), and the time average of *F[n]* over six minutes was calculated to obtain a proportional estimate of the CO estimate. Thus, the algorithm presented here provides a comprehensive set of cardiovascular indices (ABF, SV, CO, and *τ*) based on an analysis of ABP waveforms.

B. Implementation

Onset and peak of systole

For each beat, the onset and peak of systole were identified in the following manner. First, a normalized Gaussian distribution (width=4σ) was prepared. For the first iteration, the width was arbitrarily set to 75 samples. Secondly, the Gaussian distribution was convoluted with the 10-second ABP signal. Thirdly, the local maxima of the convolution waveform were identified. Next, the time stamps of the local maxima were mapped on the original ABP signal, and the closest local maxima around the time stamp were regarded as systolic peaks. Once the systolic peaks were identified, the local minima prior to the peaks were regarded as end-diastole. For the following 10-second ABP signals, the width of the Gaussian distribution was updated by

4σ=RR interval.

(a) Gaussian distribution

(b) ABP signal (gray) and convolution curve (black)

Fig. 3. Determination of systolic peaks

Onset of diastole

The onset of diastole and length of diastole in each beat were obtained from the analysis of the measured ABF waveform; in each beat, the first local minimum after the systolic peak was regarded as the onset of diastole. The ABF diastolic interval in each beat was mapped onto the ABP waveforms (Fig. 4).

Fig . 4. Mapped onsets of systole and diastole from the ABF signal to the RAP signal.

However, the onset of diastole is not always available clinically. Regarding estimation of diastolic onset, Weissler et al (1963). showed that the systolic duration of the present beat is an exponential function of the preceding RR interval (14). Using pilot Yorkshire swine data sets, the following equation was adopted to estimate systolic duration that was used to identify the onset of diastole:

$$Sys_i = 436\left(1 - \exp\left(-0.0057\, RR_{i-1}^{measured}\right)\right) \quad (11)$$

where Sys is the systolic duration [samples] and RR is the RR interval [samples]. Regular baroreflex and autonomic nervous system are assumed. In the Results section, the results using the true onset of diastole and the estimated onset of diastole using Eq. 11 are reported.

Conditioning of data

To increase the robustness of the AR coefficient estimation, the original ABP data were horizontally and vertically scaled so that all the beats in the 17-beat moving window had the same systolic ABP, diastolic ABP, and RR interval as those of the middle beat in the window (i.e., ninth beat). Note that this data conditioning was conducted solely for the purpose of the AR coefficient estimation. Once the AR coefficients were obtained, the algorithm was applied to the original ABP waveform in the middle (9th beat) of the 17-beat window. The moving window was shifted on a beat-to-beat basis.

C. Experimental protocol

To validate the algorithm, previously reported (11) data from six Yorkshire swine (30–34 kg) recorded under a protocol approved by the MIT Committee on Animal Care were processed and analyzed offline. ABF was recorded using an ultrasonic flow probe (T206 with A-series probes, Transonic Systems, Ithaca, NY) placed around the aortic root. A micromanometer-tipped catheter (SPC 350, Millar Instruments, Houston,

TX) was fed retrograde to the thoracic aorta from the femoral artery for central ABP (CAP) measurement. Radial ABP (RAP) and femoral ABP (FAP) were measured using an external pressure transducer (TSD104A, Biopac Systems, Santa Barbara, CA). ABF and ABPs were recorded using an A/D conversion system (MP150WSW, Biopac Systems) at a sampling rate of 250 Hz and 16-bit resolution. For more details of the data acquisition, please refer to Mukkamala *et al.* (11). A wide range of physiological conditions was obtained by means of the administration of vaso-active drugs including phenylephrine, nitroglycerin, dobutamine, and esmolol. Table I provides a summary of the cardiovascular indices of the swine data sets.

TABLE I

Summary of Cardiovascular Indices of the Six Swine Data Sets

D. Data analysis

All the signal processing and analyses were conducted using MATLAB R2009a. The standard deviation (SD), skewness, and kurtosis of estimated systolic ABF waveforms were compared to those of the measured waveforms. The SD, skewness and kurtosis are given by

$$\sigma = \sqrt{E\left[(F_S - \mu)^2\right]} \tag{12a}$$

$$skewness = E\left[(F_S - \mu)^3/\sigma^3\right] \tag{12b}$$

$$kurtosis = E\left[(F_S - \mu)^4/\sigma^4\right] \tag{12c}$$

where F_S is the ABF (measured or estimated) of a single beat; n is the length of F_S; μ and σ are the mean and SD of F_S, respectively; and $E[.]$ represents the expected value. The SD, skewness, and kurtosis of the measured and estimated ABF were calculated on a beat-to-beat basis. For comparison, the SD, skewness, and

kurtosis of the ABP estimated using the standard Windkessel model were also computed. The proportional ABF using the Windkessel model was estimated as follows:

$$F/C_a = dP/dt + P/\tau \quad (13)$$

where τ was estimated from an exponential decay fitted to the measured diastolic ABP waveforms.

The errors in SD, skewness and kurtosis were defined as the difference between the values obtained from the estimated ABF compared to the measured ABF. The errors obtained using the algorithm and the Windkessel model were compared by means of the Mann-Whitney U test.

For comparing the estimated and measured SV and CO, the proportionality constant C_a in each animal was calculated by

$$C_a = mean(CO_{meas})/mean(CO_{est}) \quad (14)$$

where CO_{meas} and CO_{est} are the measured and estimated CO, respectively. Although C_a declines with age (10), C_a is nearly constant on the time scale of months over a wide pressure range (2, 6); thus, C_a was assumed to be constant (equal to the mean measured CO divided by the mean estimated CO) throughout the experimental period in each animal, and the SV and CO estimates were scaled by the constant in each animal to compare estimated with measured values. The root normalized mean square error (RNMSE) was used as the error measure for SV and CO:

$$RNMSE = 100\sqrt{\sum_{n=1}^{N} \{(Meas - Est)/Meas\}^2 \Big/ (N - N_f)} \quad (15)$$

where *Meas* and *Est* are the measured and estimated values, respectively; N is the number of data points; and N_f is the number of free parameters (i.e., C_a for each animal).

In the present study, the onsets of diastole were determined from the measured ABF. These onsets have to be estimated when only ABP is known. To test the sensitivity of the algorithm to errors in diastolic onset, the time stamp of the onset of diastole was offset from its actual location by ± 10% of the diastolic interval, and the RNMSEs in SV and CO estimation were calculated.

Results

Over 60,000 beats were processed and analyzed for ABF and SV, and over 110 six-minute windows were

processed and analyzed for CO. Figure 3 shows the examples of the ABF waveforms estimated from ABP

waveforms with the true onset of diastoles given. The estimated ABF is of very similar morphology and

follows the trend of the measured ABF (Fig. 5a-f). The ABF waveforms estimated by the algorithm had

smaller offsets in the SD (Fig. 6a-c), skewness (Fig. 6d-f), and kurtosis (Fig. 6g) errors than the results by the

Windkessel model (Fig. 6) except for the femoral and radial kurtosis errors. The algorithm achieved

RNMSEs of 12.7% (15.3%) in CO (SV) derived from CAP, 15.2% (19.6%) from FAP, and 15.8% (21.8%)

from RAP (Fig. 7), respectively. The errors were lower than those from the Windkessel model that achieved

17.0% (23.7%), 16.6% (18.8%), 44.8% (33.7%) RNMSEs using CAP, FAP, and RAP, respectively.

(a)   (b)   (c)

(d)   (e)   (f)

Fig. 5. Measured and computed ABF waveforms from central ABP (CAP), femoral ABP (FAP), and radial ABP (RAP) by the algorithm applied to the Swine #5 data. Nitroglycerin was administered.

The computed ABF follows the trend of the measured ABF (a-c). The estimated beat-to-beat systolic ABF waveforms present similar SD, skewness, and kurtosis trends to those of the measured waveforms (d-f).

(a) SD error histograms   (b) SD error histograms (FAP)   (c) SD error histograms (RAP)

(d) Skewness error histograms (CAP) (e) Skewness error histograms (FAP) (f) Skewness error histograms (RAP)

(g) Kurtosis error histograms (CAP) (h) Kurtosis error histograms (FAP) (i) Kurtosis error histograms (RAP)

Fig. 6. Histograms of the standard deviation (a-c), skewness (d-f) and kurtosis (g-i) errors (measured - estimated) by the algorithm (white) and the Windkessel model (black).

The value above each histogram indicates the mean of the histogram. The algorithm had smaller errors than the Windkessel model (* P<0.05) except for kurtosis for ABF derived from FAP and RAP.

(a) CO estimates from CAP (b) CO estimates from FAP   (c) CO estimates from RAP

(d) SV estimates from CAP

(e) SV estimates from FAP

(f) SV estimates from RAP

Fig. 7. Agreement of the measured and estimated SV and CO using CAP, FAP, and RAP in the six Yorkshire swine data sets.

The gray and black lines represent measured and estimated values, respectively.

(a) Windkessel ABF from CAP   (b) Windkessel ABF from FAP

(c) Windkessel ABF from RAP

Fig. 8. Examples of the ABF waveforms estimated by the simple Windkessel model using CAP (a), FAP (b), and RAP (c).

With the estimated onset of diastole (Eq. 11), the algorithm achieved RNMSEs of 13.7% (20.0%) in CO (SV) derived from CAP, 15.2% (22.9%) from FAP, and 16.7% (25.9%) from RAP, respectively. The SD, skewness, and kurtosis presented smaller errors than those from the Windkessel model.

A sensitivity analysis regarding the onsets of diastoles was conducted. With the diastolic intervals increased by 10%, the CO (SV) estimation errors increased by 0.5 (3.9%), 4.0% (6.1%), and 3.7 (2.3%) using CAP, FAP, and RAP, respectively. With diastolic intervals decreased by 10%, the errors increased by 3.4% (10.5%), 4.4% (4.7%), and 7.8% (6.2%), respectively. For both the ± 10% cases, the SD, skewness, kurtosis errors were hardly changed compared with the values reported in Fig. 6.

Discussion

We have introduced a novel algorithm to continuously estimate ABF, SV, and CO from the analysis of central and peripheral ABP waveforms. As opposed to the existing pulse contour methods (PCMs) that also analyze ABP to calculate CO and SV (1, 3-5, 7, 9, 11-13), the present method reconstructs more fundamental information, i.e., instantaneous ABF across the aortic valve that is used to calculate CO and SV. The method estimates ABF within a proportionality constant of C_a and does not require demographical data, as opposed to the existing methods (8, 15).

The algorithm utilizes the notion that the flow input to the arterial system is zero during diastole. In the ABF estimation routine, 17 diastolic ABP waveforms were used in the left-hand side of Eq. 4 to obtain the AR coefficients (Fig. 2a). The AR coefficients and the derived weighting coefficient α were integrated into the ARX model (Fig. 1) and applied to the entire ABP waveform of the middle beat to obtain the ABF waveform. The AR coefficients were also used to obtain the impulse response (Fig. 2b) and characteristic time constant τ (Eq. 8) to properly scale the estimated ABF (Eq. 10). Note that the impulse response also includes the fast time constant that is associated with aortic resistance and arterial compliance) shown as a rapid decay between 0 - 0.2 seconds in Fig. 2b. These descriptors are comprehensively incorporated in the ARX model.

The conditioning of the data to synthesize the systolic and diastolic ABP within the moving window was conducted. Without conditioning, instability in the impulse response and noisiness in the estimated ABF waveforms were observed. We found that the cause of the estimated impulse response instability was beat-to-beat variations in ABP. The instability could be removed by rescaling the amplitude and duration of the ABP waveform of each beat in the window prior to estimating the AR coefficients. The derived AR coefficients were applied to the original ABP waveform of the middle beat to obtain ABF.

The 17-beat moving window size was empirically chosen; if the window is too short, one cannot excite

enough modes to identify the system. On the other hand, if the window is too long, time-invariance of the pertinent cardiovascular system cannot be assumed (e.g., baroreflex feedback changes of TPR and τ).

To determine the AR coefficient length L, we minimized $\Sigma a[j]$ because the resulting sets of AR coefficients were most likely to result in a stable impulse response $h[n]$. In cases where there were multiple local minima of $\Sigma a[j]$ in the search space, the minimum with the shortest AR coefficient length L was adopted.

The algorithm achieved 12.7-15.8% (15.3-21.8%) CO (SV) RNMSEs with the true onset of diastole given, and 13.7-16.7% (20.0% - 25.9%) RNMSEs with the estimated onset of diastole using Eq. 11. For both of the cases, The ABF estimated by the algorithm provided SD, skewness and kurtosis values that matched those of the measured ABF waveforms.

The sensitivity analysis regarding the onsets of diastole indicates that the error in estimating SV and CO was greater when the diastolic interval was shortened than when it was lengthened. This may be due to the fact that the diastolic decay is more rapid in early diastole and the loss of this information in estimating the AR coefficients adversely affects the accuracy of the method.

The classical Windkessel model assumes an exponential decay during diastole and thus represents a first-order AR model. The Windkessel model results in an early systolic peak (also indicated by the left shift of the skewness error histogram, Fig. 6d-f in black) in the estimated ABF waveforms, as shown in Fig. 8. The present algorithm, on the other hand, obtains higher-order AR coefficients (Fig. 4a) from diastolic ABP waveforms. The advantage of the new algorithm is that it may take into account the possible distortion involved in the diastolic ABP waveform that results from its propagation through the arterial tree. Therefore, when applied to the systolic ABP, the filter created by the algorithm may compensate for the distortion and more accurately reconstruct the systolic ABF waveform (Fig. 5). The distortion varies from artery to artery, as well as from subject to subject. The algorithm is able to measure and correct for such distortion.

The present algorithm is easy to implement in existing medical systems that continuously monitor ABP. The ABF waveform, CO, and SV estimated by the analysis of ABP waveforms may enable multi-modal

evaluation of the cardiovascular system in clinical and ambulatory settings.

Conclusion

This paper has introduced a novel algorithm that estimates ABF waveforms by the analysis of ABP waveforms. The algorithm uses diastolic ABP waveforms in a 17-beat moving window to obtain AR coefficients as well as the characteristic time constant. The AR coefficients are used in the ARX model to estimate ABF waveforms. Integrals and time averages were taken to calculate beat-to-beat SV and CO values.

The algorithm was applied to six Yorkshire swine data sets encompassing a wide physiological range, and it achieved low RNMSEs in CO (12.7-15.8%) and SV (15.3-21.8%) estimation when the true onset of diastole was given. With the estimated onset of diastole, it achieved low RNMSEs in CO (13.7-16.7%) and SV (20.0% - 25.9%) estimation. The estimated ABF waveforms accurately track features of the measured ABF waveforms.

Acknowledgment

References

1. **Arai T, Lee K, and Cohen RJ**. A novel algorithm to continuously monitor change of total peripheral resistance using peripheral arterial blood pressure values for prediction of orthostatic intolerance. In: *International Astronautical Congress*. Glasgow, Scotland: 2008, p. IAC-08.A01.02.13.

2. **Bourgeois MJ, Gilbert BK, Donald DE, and Wood EH**. Characteristics of aortic diastolic pressure decay with application to the continuous monitoring of changes in peripheral vascular resistance. *Circ Res* 35: 56-66, 1974.

3. **Bourgeois MJ, Gilbert BK, Von Bernuth G, and Wood EH**. Continuous determination of beat to beat stroke volume from aortic pressure pulses in the dog. *Circ Res* 39: 15-24, 1976.

4. **Burkhoff D, Alexander J, Jr., and Schipke J**. Assessment of Windkessel as a model of aortic input impedance. *Am J Physiol* 255: H742-753, 1988.

5. **Cerutti C, Gustin MP, Molino P, and Paultre CZ**. Beat-to-beat stroke volume estimation from aortic pressure waveform in conscious rats: comparison of models. *Am J Physiol Heart Circ Physiol* 281: H1148-1155, 2001.

6. **Hallock P, and Benson IC**. Studies on the Elastic Properties of Human Isolated Aorta. *J Clin Invest* 16: 595-602, 1937.

7. **Herd JA, Leclair NR, and Simon W**. Arterial pressure pulse contours during hemorrhage in anesthetized dogs. *J Appl Physiol* 21: 1864-1868, 1966.

8. **Langewouters GJ, Zwart A, Busse R, and Wesseling KH**. Pressure-diameter relationships of segments of human finger arteries. *Clin Phys Physiol Meas* 7: 43-56, 1986.

9. **Liljestrand G, and Zander E**. Vergleichende Bestimmung des Minutenvolumens des Herzens beim Menschen mittels der Stickoxydulmethode und durch Blutdruckmessung. *Zeitschrift fur die gesamte experimentelle Medizin* 59: 105-122, 1928.

10. **Mohiuddin MW, Laine GA, and Quick CM**. Increase in pulse wavelength causes the systemic arterial tree to degenerate into a classical windkessel. *Am J Physiol Heart Circ Physiol* 293: H1164-1171, 2007.

11. **Mukkamala R, Reisner AT, Hojman HM, Mark RG, and Cohen RJ**. Continuous cardiac output monitoring by peripheral blood pressure waveform analysis. *IEEE Trans Biomed Eng* 53: 459-467, 2006.

12. **Parlikar T, Heldt T, and Verghese G**. Cycle-Averaged Models of Cardiovascular Dynamics. *IEEE Trans Circuit and Systems* 53: 2459-2468, 2006.

13. **Parlikar TA**. Modeling and Monitoring of Cardiovascular Dynamics for Patients in Critical Care. In: *Department of Electrical Engineering and Computer Science*. Cambridge: Massachusetts Institute of Technology, 2007.

14. **Weissler AM, Harris LC, and White GD**. Left Ventricular Ejection Time Index in Man. *J Appl Physiol* 18: 919-923, 1963.

15. **Wesseling KH, Jansen JR, Settels JJ, and Schreuder JJ**. Computation of aortic flow from pressure in humans using a nonlinear, three-element model. *J Appl Physiol* 74: 2566-2573, 1993.

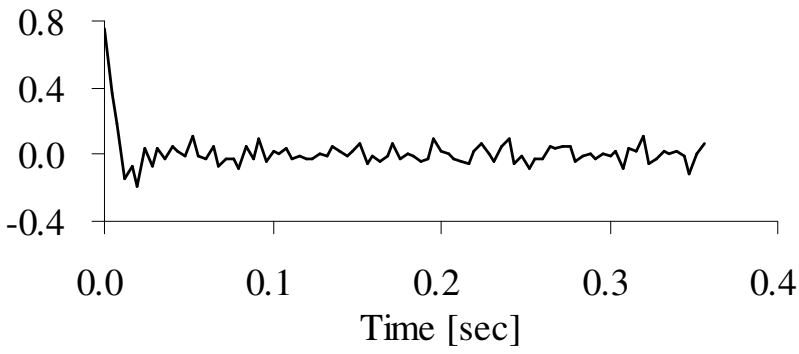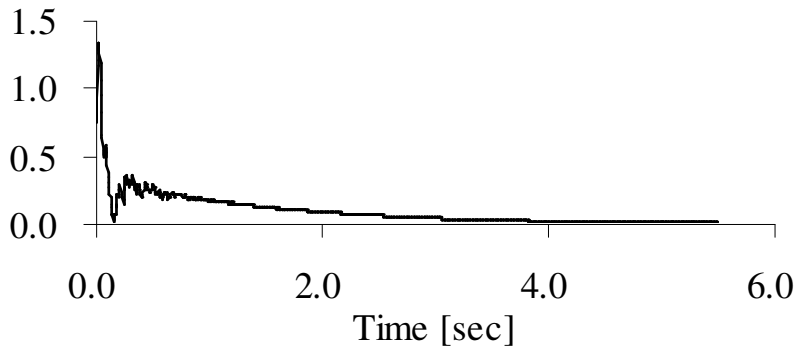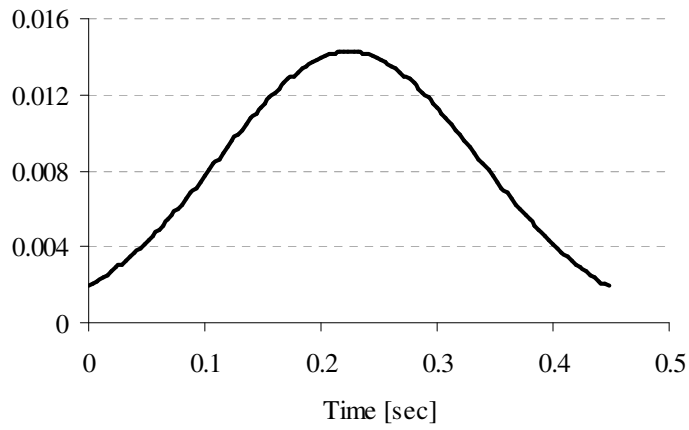**ABF [L/min]**　　　　　　　　　　　　　　　**ABP [mmHg]**

ARX

Fig. 1. ARX model.

(a) AR coefficients

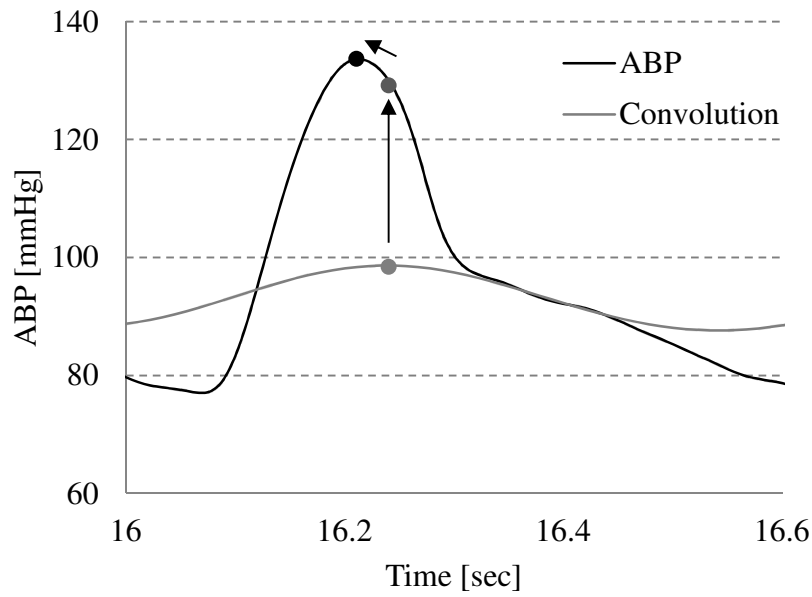

(b) Impulse response

Fig. 2. Typical AR coefficients a[j] obtained by the algorithm (a) and impulse response h[n] (b) obtained by (8) using the portion of the RAP signal in Swine #4.

(a)   Gaussian distribution

(b) ABP signal (gray) and convolution curve (black)
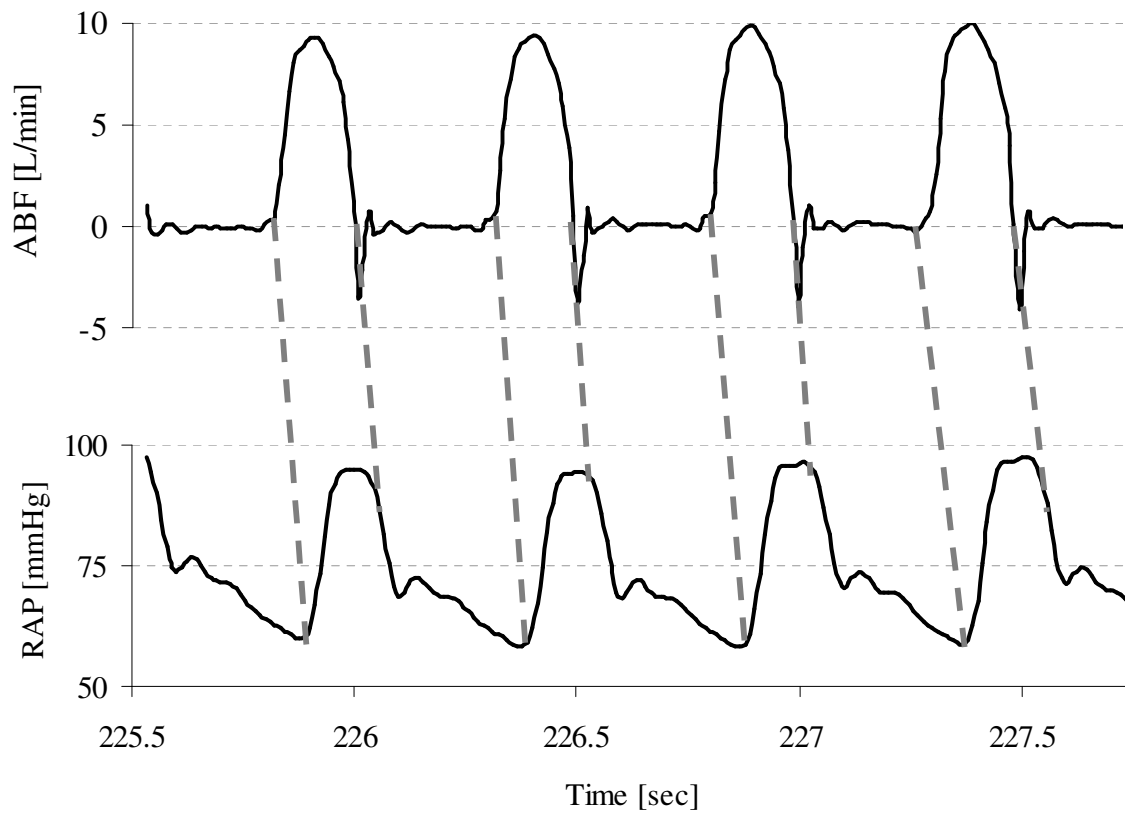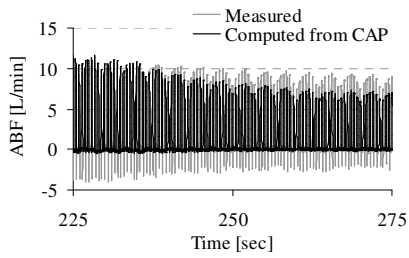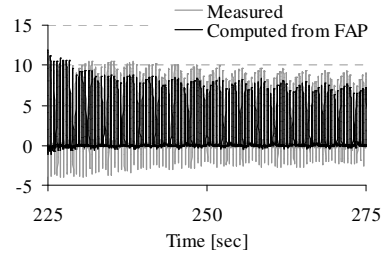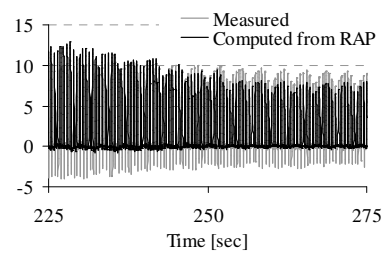
Fig. 3. Determination of systolic peaks

Fig . 4. Mapped onsets of systole and diastole from the ABF signal to the RAP signal.
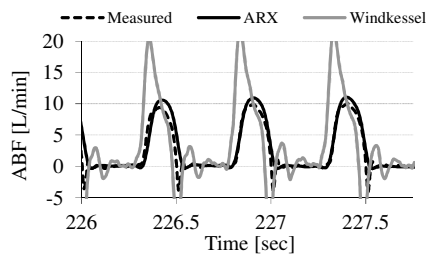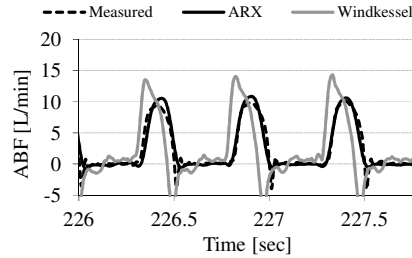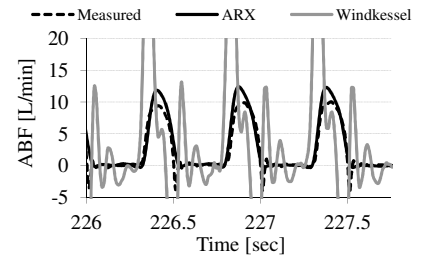
Fig. 5. Measured and computed ABF waveforms from central ABP (CAP), femoral ABP (FAP), and radial ABP (RAP) by the ARX and Windkessel algorithms applied to the Swine #5 data. Nitroglycerin was administered.
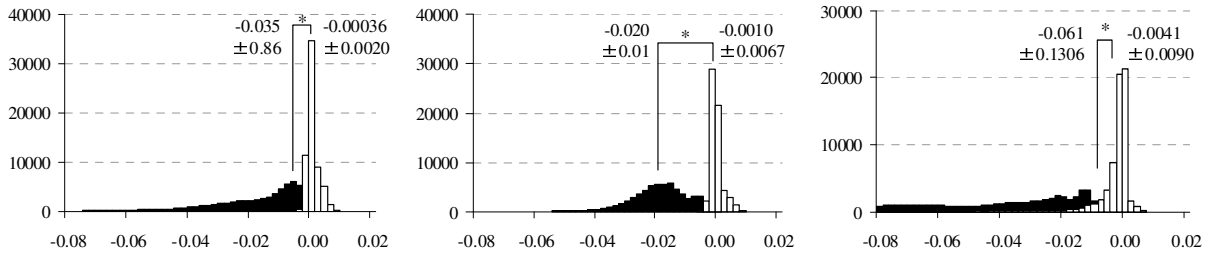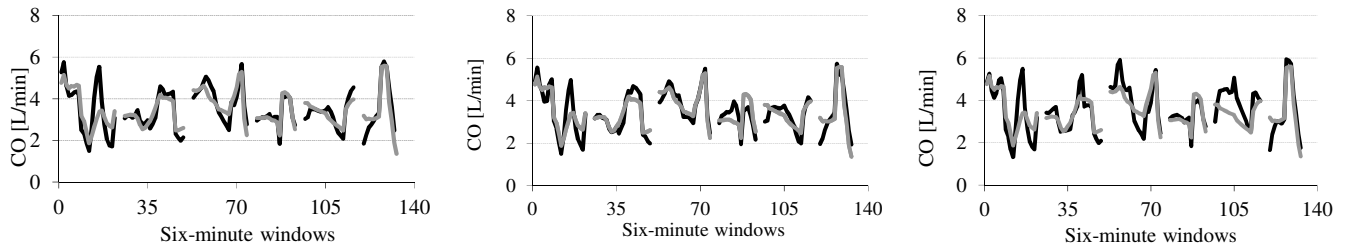
(a) SD error histograms   (b) SD error histograms (FAP)   (c) SD error histograms (RAP)
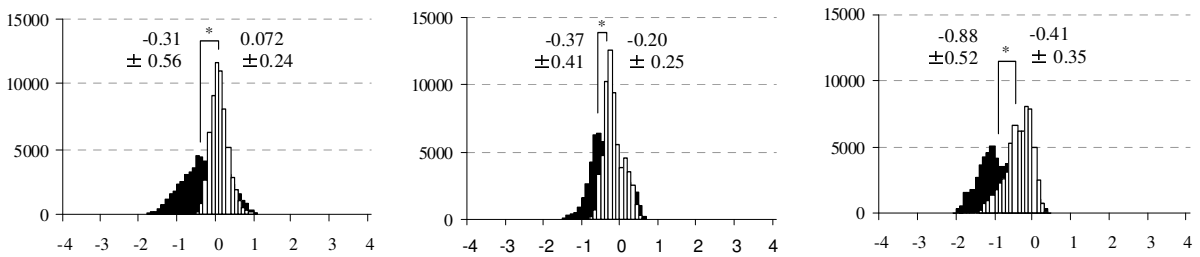
(d) Skewness error histograms (CAP) (e) Skewness error histograms (FAP) (f) Skewness error histograms (RAP)
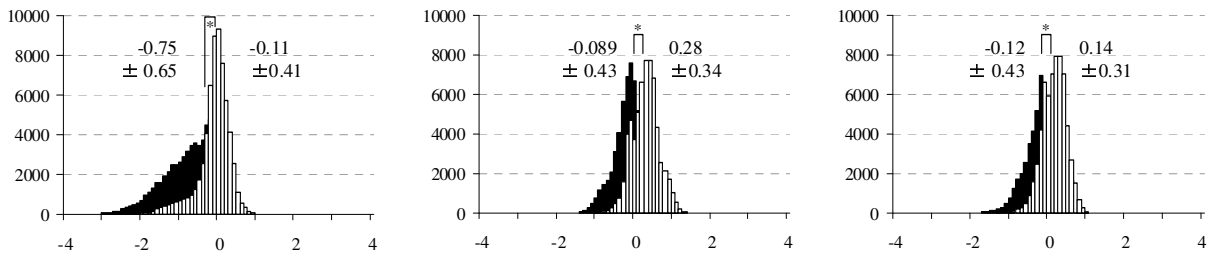
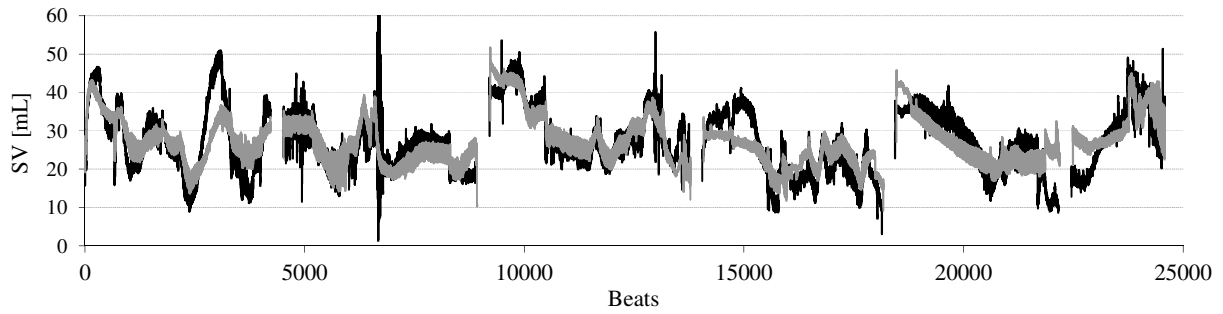(g) Kurtosis error histograms (CAP) (h) Kurtosis error histograms (FAP) (i) Kurtosis error histograms (RAP)

Fig. 6. Histograms of the standard deviation (a-c), skewness (d-f) and kurtosis (g-i) errors (measured - estimated) by the algorithm (white) and the Windkessel model (black).
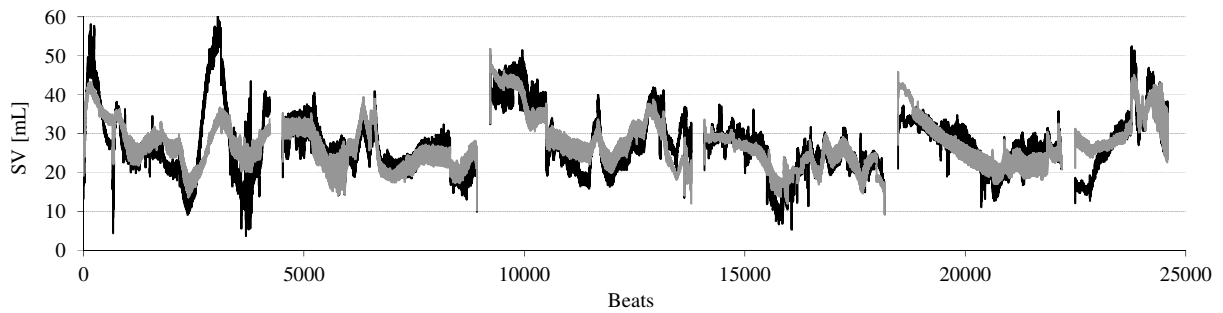
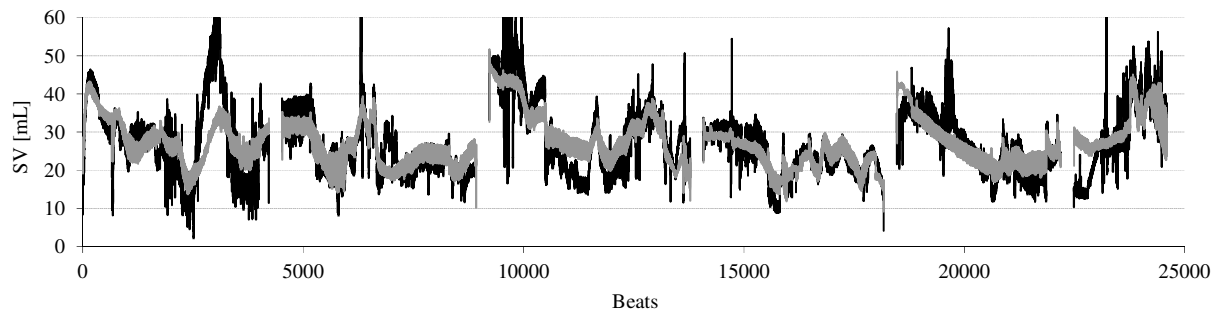(a) CO estimates from CAP   (b) CO estimates from FAP   (c) CO estimates from RAP
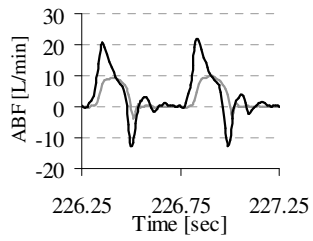

(d) SV estimates from CAP
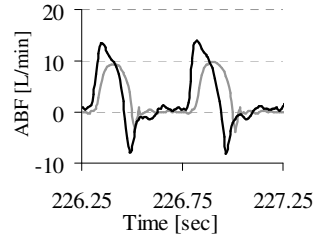

(e) SV estimates from FAP
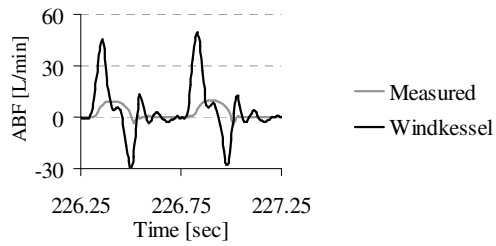

(f) SV estimates from RAP

Fig. 7. Agreement of the measured and estimated SV and CO using CAP, FAP, and RAP in the six Yorkshire swine data sets. The gray and black lines represent measured and estimated values, respectively.

(a) Windkessel ABF from CAP   (b) Windkessel ABF from FAP

(c) Windkessel ABF from RAP

Fig. 8. Examples of the ABF waveforms estimated by the simple Windkessel model using CAP (a), FAP (b), and RAP (c).

TABLE I

Summary of Cardiovascular Indices of the Six Swine Data Sets

ANIMAL	Length (min)	CO (L/min)	SV (mL)	Femoral MAP (mmHg)	Radial MAP (mmHg)	HR (bpm)
1	113	3.6 +/- 1.0	28.4 +/- 5.8	63 +/- 19	61 +/- 19	129 +/- 29
2	97	3.2 +/- 0.6	25.0 +/- 5.0	83 +/- 21	73 +/- 20	135 +/- 38
3	88	4.0 +/- 0.7	31.7 +/- 7.1	83 +/- 16	87 +/- 15	133 +/- 32
4	106	3.2 +/- 0.6	25.2 +/- 4.3	89 +/- 19	79 +/- 18	129 +/- 34
5	90	3.3 +/- 0.5	26.7 +/- 6.4	80 +/- 21	85 +/- 19	130 +/- 32
6	68	3.4 +/- 1.2	28.5 +/- 8.1	72 +/- 19	75 +/- 20	130 +/- 26
MEAN	94	3.5 +/- 0.8	27.5 +/- 6.7	79 +/- 21	76 +/- 21	131 +/- 32

Wide physiological ranges (mean ± SD) of CO, SV, femoral and radial mean arterial blood

pressure (MAP), and heart rate (HR) were achieved in the six swine data sets.